

Template synthesis of microporous carbon for direct methanol fuel cell application

Fabing Su, Jianhuang Zeng, Yaoshan Yu, Lu Lv, Jim Yang Lee, X.S. Zhao *

Department of Chemical and Biomolecular Engineering, National University of Singapore, 10 Kent Ridge Crescent, Singapore 119260, Singapore

Received 17 December 2004; accepted 16 April 2005

Available online 24 June 2005

Abstract

Ordered microporous carbon with a structure of amorphous carbon core and graphitic carbon shell was prepared using hydrogen-form zeolite Y as the template. Impregnation and chemical vapor deposition methods were employed to infiltrate carbon in the pores of the template. Physical adsorption of nitrogen, X-ray diffraction, thermogravimetric analysis, field-emission scanning electron microscope, and field-emission transmission electron microscope techniques were employed to study the structural and morphological properties of the samples. The electrochemical properties of Pt supported on the carbon samples were examined and compared with a commercial catalyst. It was observed that Pt catalyst supported on a carbon with a core/shell structure has a higher specific activity for room-temperature methanol oxidation than the commercial catalyst.

© 2005 Elsevier Ltd. All rights reserved.

Keywords: Porous carbon; Chemical vapor deposition; Porosity; Electrochemical properties

1. Introduction

Recently, template synthesis has been employed to prepare a range of porous carbons [1–5]. Highly ordered macroporous carbon materials were fabricated with colloidal crystal spheres as the template [6,7]. The preparation of ordered mesoporous carbons was widely demonstrated with different ordered mesoporous silicas (MCM-48, SBA-15, SBA-1, HMS) as the templates [2–5]. With regard to template synthesis of ordered microporous carbons, some of the previous studies ended up with disordered microporous carbons [8–12] except for Kyotani's group, who first reported the observation of structural ordering in zeolite-templated microporous carbons [13–16]. Because of many prominent characteristics [1–5], such as high surface area, relatively uniform pore size, ordered pore structure, interconnected pore

network, graphitic pore wall, tailorable surface properties, and good thermal and mechanical stability, these template-synthesized porous carbons may find applications as catalyst supports [7,17], electrochemical materials [18,19], adsorbents [20], optical materials [6], and templating matrixes for the fabrication of nanostructures [21]. As electrode or support materials, some of these new porous carbons have displayed their optimum catalytic performances in electrochemical applications such as fuel cells [7], Lithium ion batteries [18], and electrochemical capacitors [19].

As one member of the fuel cell family, direct-methanol fuel cell (DMFC) has recently attracted great attention for its future potential as clean and ideal portable power sources [22]. Carbon materials such as glassy carbon, carbon black, carbon fibers, pyrolytic graphite and highly ordered pyrolytic graphite have been used as the working electrode in electrocatalysis [23]. Recent research results have shown that the pore structure [7], surface area [24], graphitic nature [25], and surface chemistry [26] of a carbon support have a significant

* Corresponding author. Tel.: +65 68744727; fax: +65 67791936.
E-mail address: chezxs@nus.edu.sg (X.S. Zhao).

influence on the catalytic activity of electrooxidation of methanol.

In this work, template synthesis and chemical vapor deposition (CVD) were employed to fabricate ordered microporous carbon with a core/shell structure. The catalytic performance of the carbon as a Pt catalyst support for room-temperature DMFC was examined and compared with a commercial catalyst of E-TEK, which is a Pt catalyst supported on Vulcan XC-72 carbon black having a specific surface area of 220 m²/g.

2. Experimental

2.1. Template synthesis of porous carbons

Hydrogen-form zeolite Y (HY) (commercially known as CBV400 with a SiO₂/Al₂O₃ of 5.1, Zeolyst International Company) was used as the template because it is believed that the acidic sites of HY would promote polymerization/carbonization of carbon precursor furfuryl alcohol (FA). To prepare carbons with impregnation method [12], HY was first dried at 200 °C for 4 h before mixing with FA (98%, ACROS ORGANICS, USA) with a ratio of 4 cm³ of FA to 1 g of HY. After stirring at room temperature for 72 h, the solid was filtrated off, briefly washed with mesitylene (≥98%, Fluka) to remove residual furfuryl alcohol on the external surface of HY particles, and air-dried. The solid collected was placed in a quartz tube and carbonized at 900 °C with a heating rate of 2 °C/min for a holding time 4 h under highly pure N₂ flow (99.9995%, 30 cm³/min) to yield a zeolite/carbon composite. The composite was dissolved in 46% HF solution at room temperature for 24 h to remove the zeolite template. Finally, after washing and drying, a carbon sample was obtained. Here, zeolite/carbon composite was named as ZCF900-4 and carbon was designed as CF900-4, where Z, C and F represent zeolite, porous carbon and FA precursor, respectively. To prepare carbons with a combined method of impregnation and CVD, similarly, above solid collected was heated up to 900 °C in the pure nitrogen atmosphere. Subsequently, the carbonization at this temperature for 4 h was conducted under N₂ flow (30 cm³/min) containing around 10 wt.% benzene vapor derived from a liquid bubbler instead of highly pure N₂ flow. After same post-treatment, porous carbon was assigned as CFB900-4, where B stands for CVD of benzene. Similarly, the composite before washing with HF solution was donated as ZCFB900-4.

2.2. Characterization methods

The structures of the resultant porous carbons were characterized using X-ray diffraction technique (XRD) (XRD-6000, Shimadzu, Japan) with CuK α radiation

($\lambda = 1.5418 \text{ \AA}$). Thermogravimetric analysis (TGA) was conducted on a thermogravimetric analyzer TGA 2050 (Thermal Analysis Instruments, USA) in air atmosphere with a flow rate of 100 ml/min. The microscopic features of the samples were observed with a field-emission scanning electron microscope (FESEM) (JSM-6700F, JEOL Japan) operated at 10 kV and field-emission transmission electron microscopy (FETEM) (JEM 2010F, JEOL, Japan) operated at 200 kV. The porous properties of the samples were investigated using physical adsorption of nitrogen at liquid-nitrogen temperature on an automatic volumetric sorption analyzer (Quantachrome, NOVA1200). Prior to measurements, the samples were degassed at 200 °C for 5 h. The specific surface area (S_{BET}) was determined according to the Brunauer–Emmett–Teller (BET) method in the relative pressure range of 0.05–0.2. The total pore volume (V_{T}) was obtained from the volume of nitrogen adsorbed at a relative pressure of 0.95. The micropore volume (V_{mi}) was calculated from the Dubinin–Radushkevich (DR) equation.

2.3. Preparation of Pt catalyst and evaluation of electrochemical and catalytic properties

Pt catalysts supported on carbons CF900-4 and CFB900-4 with a loading of 20 wt.% were prepared using the borohydride reduction method [27], and designed as Pt/CF900-4 and Pt/CFB900-4, respectively. The preparation is described below. About 0.04 g of carbon (CF900-4 or CFB900-4) was added in a beaker containing 40 ml of distilled water under stirring. To this suspension was added 1 ml of 0.05 M chloroplatinic acid (H₂PtCl₆ · 6H₂O, Aldrich) solution. Then, stoichiometric excess (around 1 ml) of 0.5 M NaBH₄ (Aldrich) solution was added to the beaker to initiate deposition of Pt nanoparticles. After stirring for 12 h, the solid was recovered by centrifugation, extensively washed with distilled water, and vacuum-dried at room temperature overnight. The catalysts thus obtained are denoted as Pt/CF900-4 and Pt/CFB900-4, respectively.

The catalytic performance of the Pt catalysts for room-temperature methanol oxidation was investigated and benchmarked toward the commercial Pt catalyst Pt/C E-TEK (the loading of Pt is 20 wt.%). A conventional three-compartment electrochemical cell was used to evaluate the electrochemical performance by cyclic voltammetry. An Autolab PGSTAT12 served as the potentiostat/galvanostat. The working electrode was fabricated by casting Nafion-impregnated catalyst ink onto a 5-mm diameter vitreous glassy carbon disk electrode. A Pt gauze and a saturated calomel electrode (SCE) were used as the counter and the reference electrodes respectively while 0.5 M H₂SO₄ with or without 1 M CH₃OH were the electrolyte. All reported potentials were referenced to the SCE. The catalysts were

cycled between 0 and 1 V at 20 mV s^{-1} until a stable response was obtained before the cyclic voltammograms were recorded.

3. Results and discussion

3.1. XRD analysis

Shown in Fig. 1 are the XRD patterns of porous carbons synthesized under different conditions. It is seen that sample CF900-4 prepared without using CVD exhibits a broad XRD peak at around 13.4° as observed previously [12]. However, carbon CFB900-4, which was prepared with the assistance of CVD of benzene, displays a peak at about 6.2° , suggesting the presence of long-range structural ordering with a periodicity of around 1.4 nm [15]. This peak is considered to be transferred from the periodicity of zeolite HY template, demonstrating a structural replication process [14,15]. The relatively broad peak observed at about 25.3° , corresponding to (002) diffraction of graphitic carbon [25], is seen on sample CFB900-4, but not on CF900-4. Therefore, it is concluded that CVD of benzene cannot only improve the structural order but also lead to the formation of graphitic carbon, which may improve the electron conductivity of the carbon [22]. Although high CVD temperatures favor the formation of graphitic carbon [28], it was noticed that structure collapses of zeolite Y template occurred at the temperatures higher than 900°C [12].

3.2. Thermogravimetric analysis

The thermogravimetric (TG) and derivative thermogravimetric (DTG) curves of composites and carbons

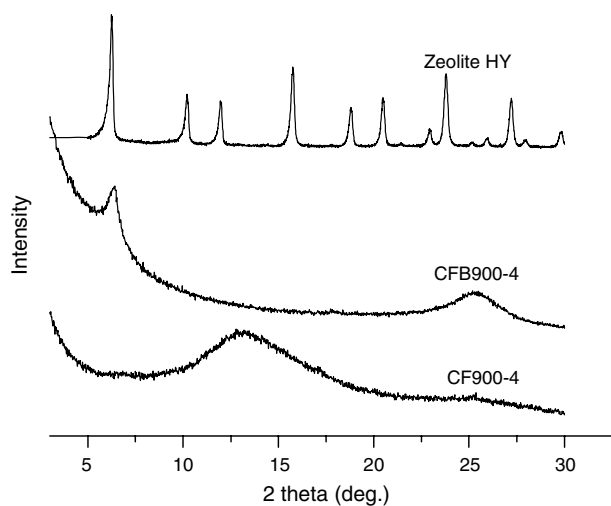


Fig. 1. XRD patterns of carbons CFB900-4 and CF900-4, and zeolite HY.

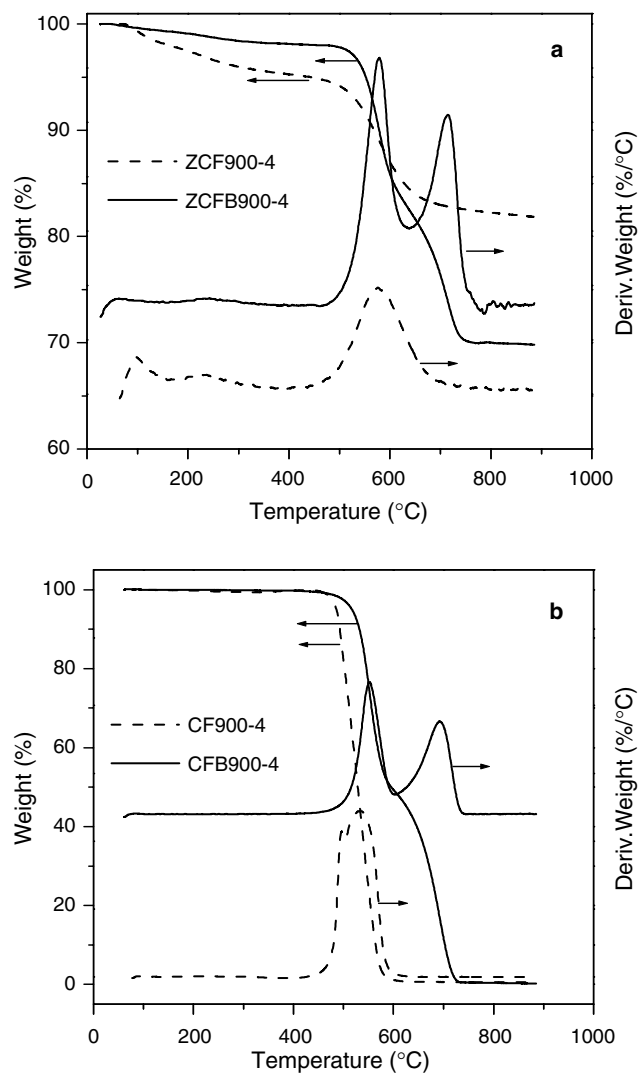


Fig. 2. TG weight loss curves and DTG curves of carbon/zeolite composites (a) and porous carbons (b) in air.

are shown in Fig. 2. Considering the TG curves shown in Fig. 2a, the weight losses of the composites below 200°C are due to the desorption of physically adsorbed water, and those between 200 and 900°C are because of carbon combustion. The residual masses after 850°C are similarly considered as the content of zeolite template in the composites [12]. The weight losses of composites ZCF900-4 and ZCFB900-4 after 850°C are calculated to be about 18 and 30 wt.%, respectively. Subtracting the weight losses due to physically adsorbed water yielded carbon content in the composites corresponds to 0.18, and 0.41 g carbon per g HY, respectively, indicating that CVD of benzene dramatically increased carbon fraction in the composites. It can be observed from DTG curves of composites in Fig. 2a that ZCF900-4 has one peak at 570°C and ZCFB900-4 reveals two peaks centered at 570°C and 715°C . The similarly peaks also are seen in Fig. 2b DTG curves of resulting carbon samples CF900-4 and CFB900-4.

Before thermal analysis, the carbon samples were dried at 150 °C over night to eliminate physically adsorbed water. The key information from the TG curves of carbons shown in Fig. 2b is that the zeolite template was completely dissolved away by aqueous HF solution because of the nearly zero residues after 800 °C for both carbon samples. It can be seen from the DTG curves that sample CF900-4 has one broad peak centered at about 500 °C. On contrast, sample CFB900-4 displays two well-resolved weight loss events: one at the temperature of about 550 °C and the other one at about 700 °C, indicating the presence of two different carbon species. With consideration of the data shown in Fig. 1, the carbon species showing a higher combustion temperature is due to graphitic carbon, and the carbon species with a lower combustion temperature is ascribed to amorphous carbon. Taking into account TGA curves of composites and resultant carbons, it is believed that the amorphous carbon was generated from the infiltrated carbon precursor in the channels of the template while the graphitic carbon was created on the external surfaces of the template particles during CVD of benzene. This conclusion is supported by the FESEM and FETEM data shown below.

3.3. Observation of FESEM

Fig. 3 shows the FESEM images of zeolite HY and the carbons. It is seen that samples CF900-4 (Fig. 3b) and CFB900-4 (Fig. 3c) preserved the morphology of the template HY particles (Fig. 3a). The rough surface observed on sample CFB900-4 (Fig. 3c and d) is an indicative of pyrolytic carbon species deposited on the external surface of the template. The rough surface may be helpful for the deposition and fixation of metal catalyst nanoparticles.

3.4. Observation of FETEM

Fig. 4 presents the FETEM photographs of the carbon samples. A homogeneous carbon framework can be seen on sample CF900-4 (Fig. 4a). A core/shell structure is obviously seen on sample CFB900-4 (Fig. 4b), which was prepared with the assistance of CVD of benzene. A dense carbon layer (around 5–10 nm) is clearly seen on the surface of the carbon core. The formation of the core/shell carbon structure is believed to be related to the preparation method. At the early stage of carbon deposition, pyrolytic carbon was deposited on the zeolite pore surface forming the carbon core carbon. After finishing infiltration of carbon in the pores, deposition of carbon on the external surface of the zeolite template occurred, resulting in the formation of the carbon shell.

A high-magnification FETEM image of carbon CF900-4 is shown in Fig. 4c. It is seen that the carbon

structure is disordered and isotropic, consisting of microporous amorphous carbon. However, sample CFB-900-4 contains both amorphous and graphitic carbons as revealed by the FESEM image shown in Fig. 4d, which was taken from a focused area with a boundary between the carbon core and shell. The core carbon in the left part of the image looks similar to the amorphous carbon shown in Fig. 4c, indicating an amorphous carbon in nature. The shell in the right part of the image displays flat graphene carbon sheets of graphitic nature [29]. Because of the small pore size of the supercages (1.4 nm) and channels (0.7 nm) of zeolite HY [30], the graphene sheets can not be formed in the pores of the template [14]. Thus, graphitic carbon was formed only on the external surface of the template.

3.5. Nitrogen adsorption

Fig. 5 shows the nitrogen adsorption/desorption isotherms of the carbon samples, together with that of zeolite HY. It is seen that the isotherms are all of type I, indicating microporous materials [31]. However, the carbon materials display a slower micropore filling step compared to zeolite HY, implying the presence of large micropores and/or mesopores.

The BET surface area and pore structure parameters determined from the nitrogen adsorption data are summarized in Table 1. It can be seen that at the same synthesis temperature (900 °C) and holding time (4 h), porous carbon CFB900-4 obtained using CVD method have a little higher surface area and pore volume than CF900-4 without using CVD, demonstrating the CVD almost has no effect on surface area and pore volume of amorphous carbon core while it can bring about ordered structure and graphitic carbon shell of CFB900-4. Additionally, these results further imply the carbon shell is very thin (also can be seen from Fig. 4b TEM image).

3.6. Pt catalysts supported on the carbon

Fig. 6 compares the TEM images of the commercial catalysts Pt/C (E-TEK) and catalyst Pt/CFB900-4. Relatively uniformly dispersed Pt nanoparticles are seen on the surfaces of both catalysts. However, the size of the Pt particles supported on carbon CFB900-4 is slightly larger than that on carbon Vulcan XC-72.

Fig. 7 shows the XRD patterns of the two catalysts. The peak at around 25° is attributed to the (002) diffraction of the graphitic structure of the carbon supports. The diffraction intensity of this peak for carbon CFB900-4 is comparable to that of carbon XC-72. The Pt nanoparticles supported on CFB900-4 exhibit an XRD pattern of a typical face-centered-cubic (fcc) lattice structure. The strong diffraction peaks at the Bragg angles of 39.8°, 46.3°, 67.5° and 81.3° correspond to the

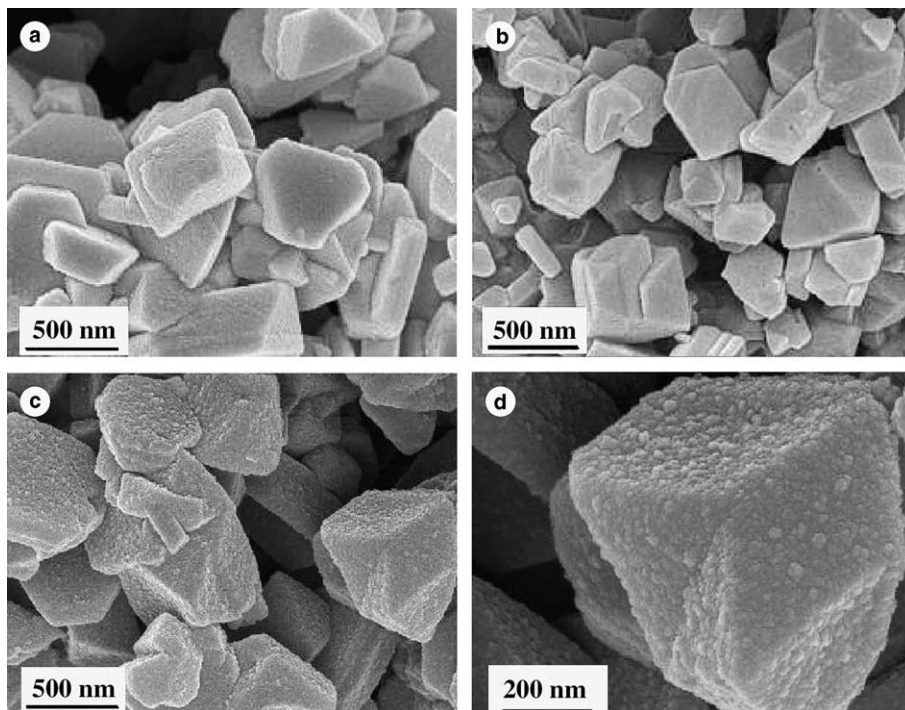


Fig. 3. FESEM images of zeolite HY (a), carbon CF900-4 (b), and carbon CFB900-4 (c, d).

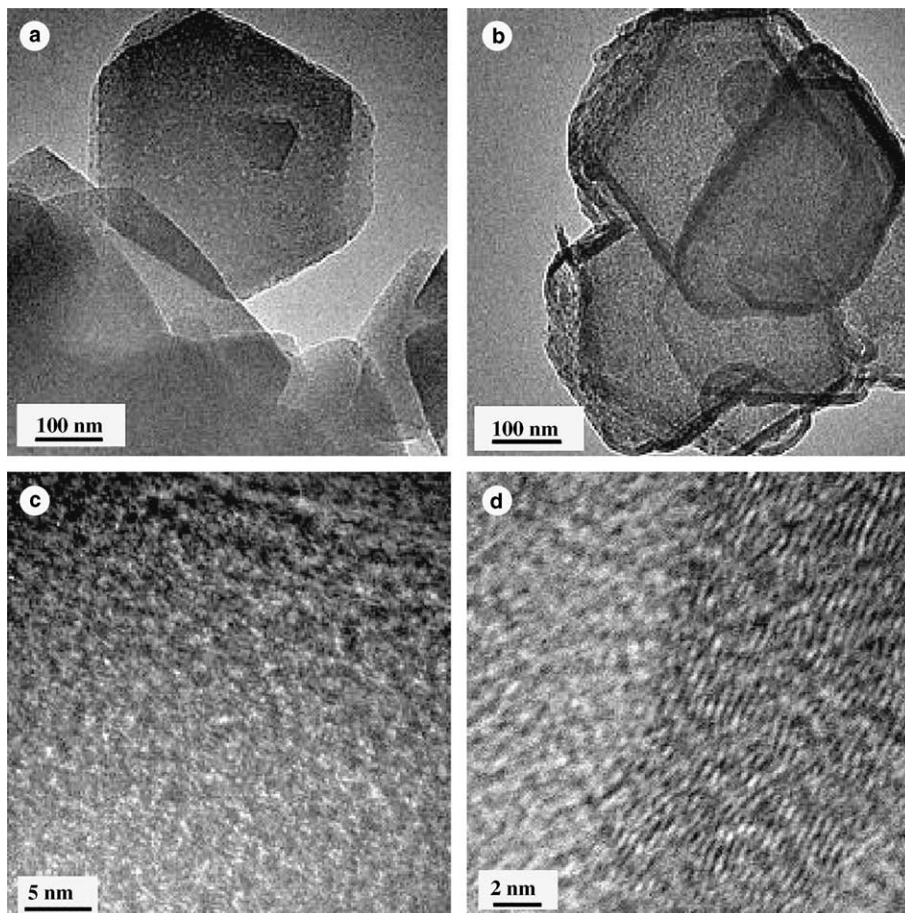


Fig. 4. FETEM images of porous carbons CF900-4 (a, c) and CFB900-4 (b, d).

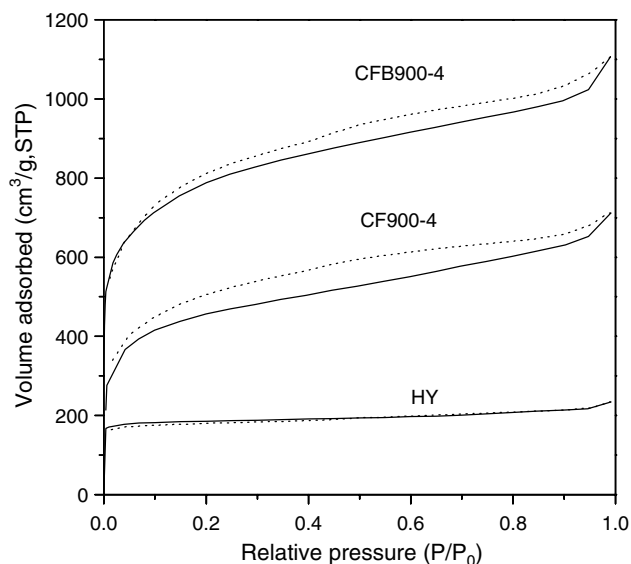


Fig. 5. Nitrogen adsorption/desorption isotherms of porous carbons and zeolite HY template (solid line: adsorption branch; dot line: desorption branch). For clarity, the isotherm of CFB900-4 was vertically shifted 300 cm³/g.

Table 1

The pore structure parameters of microporous carbons and HY template

Sample	$S_{\text{BET}}^{\text{a}}$ (m ² /g)	V_{t}^{b} (cm ³ /g)	V_{mi}^{c} (cm ³ /g)
CF900-4	1616	1.00	0.74
CFB900-4	1722	1.11	0.76
HY	648	0.34	0.29

^a BET surface area.

^b Total pore volume.

^c Micropore volume.

(111), (200), (220) and (311) facets of Pt crystal [32]. Using the Debye–Scherrer equation, the average Pt nanoparticle sizes of catalysts Pt/C and Pt/CFB900-4 were estimated to be about 3.8 and 4.7 nm, respectively, which are consistent with the observations from Fig. 6. The difference in Pt particle size between the two cata-

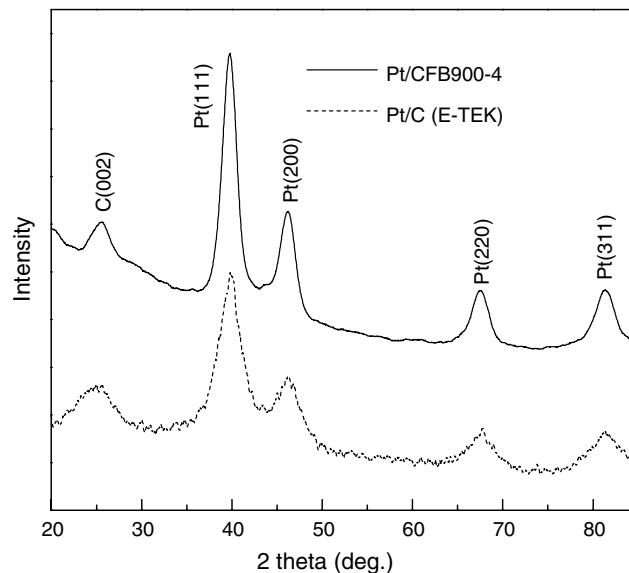


Fig. 7. XRD patterns of the Pt/C E-TEK and Pt/CFB900-4 catalysts.

lysts may be due to the different surface chemistries of the two carbon supports [22,26].

3.7. Electrochemical properties of the catalysts

Cyclic voltammetry is one of the most common techniques in electrochemical studies of fuel cell reactions. It is employed primarily as an effective way to compare electrodes on the basis of currents during a potential sweep at some arbitrary sweep rate. Fig. 8a shows the cyclic voltammograms (CV) of Pt/CFB900-4 and Pt/C E-TEK catalysts in 0.5 M H₂SO₄. Hydrogen adsorption or desorption peaks in the potential region from -0.2 V to 0.05 V are due to the presence of Pt facets. The electrochemically active surface area of the Pt catalysts can be estimated from the charges associated with hydrogen adsorption (shaded area) on Pt facets in the potential range from -0.2 to 0.05 V. Highly pure Ar was used prior to and during the measurements to deaerate the electrolyte. The straight baseline of measurements was

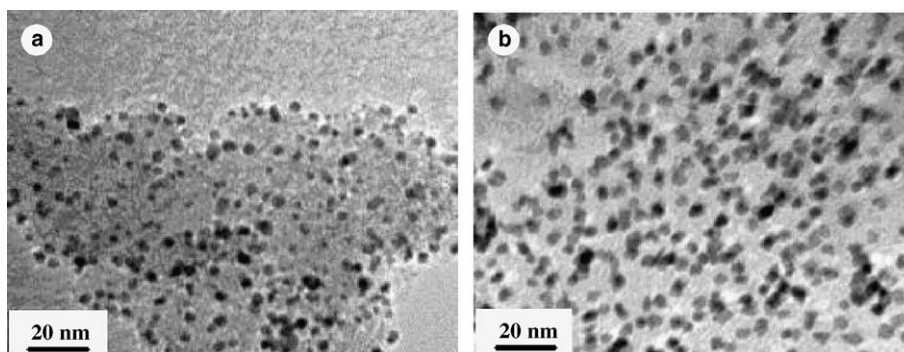


Fig. 6. TEM images of the E-TEK Pt/C catalyst (a) and Pt/CFB900-4 catalyst (b).

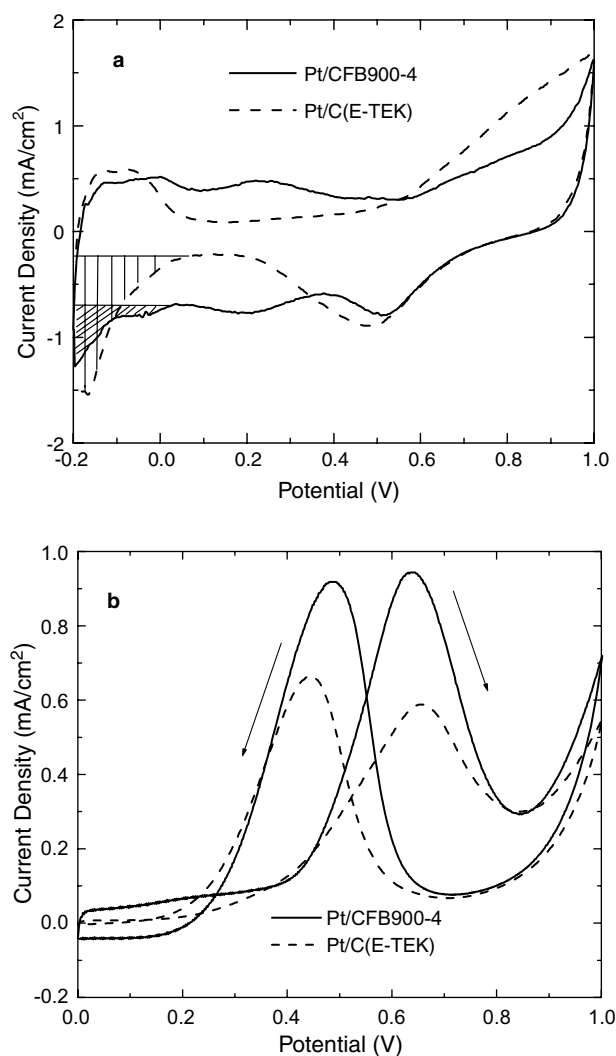


Fig. 8. Cyclic voltammograms of Pt/CFB900-4 and Pt/C (E-TEK) catalysts measured at a scan rate of 20 mV s^{-1} at room temperature in electrolytes of (a) $0.5 \text{ M H}_2\text{SO}_4$ and (b) $1 \text{ M CH}_3\text{OH} + 0.5 \text{ M H}_2\text{SO}_4$. (Forward scan: $0.0\text{--}1.0 \text{ V}$ and reverse scan: $1.0\text{--}0.0 \text{ V}$.)

extended from the double-layer region of the CV. The electrochemical surface area in m^2/g was calculated assuming a correspondence value of $0.21 \text{ mC}/\text{cm}^2$ Pt [33]. Similar to E-TEK Pt/C catalysts, the well-defined Pt facets for hydrogen adsorption/desorption observed on Pt/CFB900-4 catalyst may be attributed to the graphitic nature of the shell of carbon CFB900-4. Such Pt facets were not observed on Pt catalysts supported on amorphous carbon CF900-4 [34].

Fig. 8b shows the specific activities for room-temperature methanol oxidation of the two catalysts. The specific activity, an indication of the intrinsic activity of the Pt site, has been normalized to the electrochemical active surface areas. The anodic peak at around 0.47 V in the reverse scan can be associated with the reactivation of oxidized Pt. The current peak at about 0.63 V in the forward scan is attributed to methanol electrooxi-

dation on the Pt catalyst. Fig. 8b clearly shows that this peak is significantly higher in the Pt/CFB900-4 catalyst than in the Pt/C (E-TEK) catalyst. The specific activity of Pt/CFB900-4 catalyst, which is evaluated by the peak current value at around 0.63 V , outperformed the commercial catalyst E-TEK by about 60%. The enhanced specific activity is considered to be due to the unique core-shell structure of the ordered microporous carbon. Compared to the CF900-4, the graphitic carbon shell of CFB900-4, which had a similar graphitic nature to XC-72, offered a high electronic conductivity [22,25], a good interaction with Pt nanoparticles and a proper Pt particle size on the surface of support [22,26]. It has been reported that Pt nanoparticles form six Pt-C bonds at the metal-carbon interface on Vulcan XC-72 and four Pt-C bonds at the metal-carbon interface on oxygen-rich carbon supports such as CFB900-4 [26]. Therefore, the Pt particles in Pt/CFB900-4 are possibly more chemically active than those in Pt/C E-TEK. The pore structure of CFB900-4 carbon support may also accounts for the enhanced specific activity since the ordered microporous network with a high surface area can facilitate the transport of methanol and reaction product CO_2 gas as compared to that of XC-72 composed of randomly distributed particles with varying sizes [7,22]. However, the detailed understanding is complicated and further work is also in progress. In an attempt to measure the electroconductivity of the microporous carbons synthesized in this work, CV spectra were measured on catalyst Pt/CFB900-4 and a mix of carbon Vulcan XC-72 with catalyst Pt/CFB900-4 in a mass ratio of 1:1. It was observed that the CV spectra (not shown) in both $0.5 \text{ M H}_2\text{SO}_4$ and $1 \text{ M CH}_3\text{OH} + 0.5 \text{ M H}_2\text{SO}_4$ electrolytes were similar, indicating that the electroconductivity of carbon CFB900-4 is comparable to Vulcan XC-72. These above results show that the ordered microporous carbon CFB900-4 has a high application potential in DMFCs.

4. Conclusions

Using zeolite HY as the template, ordered microporous carbon with a core/shell structure has been prepared. Structural transformation from zeolite HY template to the resultant carbon has been realized when CVD was used to assist carbon infiltration. The microporous carbon possesses a long-range ordering with a structural regularity of 1.4 nm , matching well with the periodical pore structure of zeolite HY. The use of CVD of benzene can not only enhance carbon infiltration, but also promote the formation of the graphitic carbon shell, creating the porous carbon with an amorphous core and a graphitic shell. The specific activity of Pt catalyst supported on the core-shell carbon for room-temperature methanol oxidation has been observed to outperform a commercial catalyst Pt/C (E-TEK).

Acknowledgment

We thank NUS for financial support (grant number R279000124112). Dr. Xu Xiaojing and Mr. Shang Zhenhua are thanked for FETEM measurements.

References

- [1] Kyotani T. Control of pore structure in carbon. *Carbon* 2000;38(2):269–86.
- [2] Ryoo R, Joo SH, Kruk M, Jaroniec M. Ordered mesoporous carbons. *Adv Mater* 2001;13(9):677–81.
- [3] Schüth F. Endo- and exotemplating to create high-surface-area inorganic materials. *Adv Mater* 2003;42:3604–22.
- [4] Lee J, Han S, Hyeon T. Synthesis of new nanoporous carbon materials using nanostructured silica materials as templates. *J Mater Chem* 2004;14:478–86.
- [5] Yang H, Zhao D. Synthesis of replica mesostructures by the nanocasting strategy. *J Mater Chem* 2005;15:1217–31.
- [6] Zakhidov AA, Baughman RH, Iqbal Z, Cui C, Khayrullin I, Dantas SO, et al. Carbon structures with three-dimensional periodicity at optical wavelengths. *Science* 1998;282:897–901.
- [7] Chai GS, Shin IS, Yu J-S. Synthesis of ordered, uniform, macroporous carbons with mesoporous walls templated by aggregates of polystyrene spheres and silica particles for use as catalyst supports in direct methanol fuel cells. *Adv Mater* 2004;16(22):2057–61.
- [8] Johnson SA, Brigham ES, Ollivier PJ, Mallouk TE. Effect of micropore topology on the structure and properties of zeolite polymer replicas. *Chem Mater* 1997;9:2448–58.
- [9] Rodriguez-Mirasol J, Cordero T, Radovic LR, Rodriguez JJ. Structural and textural properties of pyrolytic carbon formed within a microporous zeolite template. *Chem Mater* 1998;10: 550–8.
- [10] Meyers CJ, Shah SD, Patel SC, Sneeringer RM, Bessel CA, Dollahon NR, et al. Templated synthesis of carbon materials from zeolite (Y, Beta, and ZSM-5) and a montmorillonite clay (K10): physical and electrochemical characterization. *J Phys Chem B* 2001;105:2143–52.
- [11] Barata-Rodrigues PM, Mays TJ, Moggridge GD. Structured carbon adsorbents from clay, zeolite and mesoporous aluminosilicate templates. *Carbon* 2003;41(12):2231–46.
- [12] Su F, Zhao XS, Lv L, Zhou Z. Synthesis and characterization of microporous carbons templated by ammonium-form zeolite Y. *Carbon* 2004;42(14):2821–31.
- [13] Ma Z, Kyotani T, Tomita A. Preparation of a high surface area microporous carbon having the structural regularity of Y zeolite. *Chem Commun* 2000:2365–6.
- [14] Ma Z, Kyotani T, Liu Z, Terasaki O, Tomita A. Very high surface area microporous carbon with a three-dimensional nano-array structure: synthesis and its molecular structure. *Chem Mater* 2001;13:4413–5.
- [15] Ma Z, Kyotani T, Tomita A. Synthesis methods for preparing microporous carbons with a structural regularity of zeolite Y. *Carbon* 2002;40(13):2367–74.
- [16] Kyotani T, Ma Z, Tomita A. Template synthesis of novel porous carbons using various types of zeolites. *Carbon* 2003;41(7): 1451–9.
- [17] Joo SH, Choi SJ, Oh I, Kwak J, Liu Z, Terasaki O, et al. Ordered nanoporous arrays of carbon supporting high dispersions of platinum nanoparticles. *Nature* 2001;412:169–72.
- [18] Zhou H, Zhu S, Hibino M, Honma I, Ichihara M. Lithium storage in ordered mesoporous carbon (CMK-3) with high reversible specific energy capacity and good cycling performance. *Adv Mater* 2003;15:2107–11.
- [19] Alvarez S, Blanco-López MC, Miranda-Ordieres AJ, Fuertes AB, Centeno TA. Electrochemical capacitor performance of mesoporous carbons obtained by templating technique. *Carbon* 2005; 43(4):866–70.
- [20] Su F, Lv L, Hui TM, Zhao XS. Phenol adsorption on zeolite-templated carbons with different structural and surface properties. *Carbon* 2005;43:1156–64.
- [21] Roggenbuck J, Tiemann M. Ordered mesoporous magnesium oxide with high thermal stability synthesized by exotemplating using CMK-3 carbon. *J Am Chem Soc* 2005;127:1096–7.
- [22] Chan K-Y, Ding J, Ren J, Cheng S, Tsang KY. Supported mixed metal nanoparticles as electrocatalysts in low temperature fuel cells. *J Mater Chem* 2004;14:505–16.
- [23] Banks CE, Davies TJ, Wildgoose GG, Compton RG. Electrocatalysis at graphite and carbon nanotube modified electrodes: edge-plane sites and tube ends are the reactive sites. *Chem Commun* 2005:829–41.
- [24] Park K-W, Sung Y-E, Han S, Yun Y, Hyeon T. Origin of the enhanced catalytic activity of carbon nanocoil-supported PtRu alloy electrocatalysts. *J Phys Chem B* 2004;108:939–44.
- [25] Hyeon T, Han S, Sung Y-E, Park K-W, Kim Y-W. High-performance direct methanol fuel cell electrodes using solid-phase-synthesized carbon nanocoils. *Angew Chem Int Ed* 2004;42: 4352–6.
- [26] Zhang Y, Toebes ML, van der Eerden A, O'Grady WE, de Jong KP, Koningsberger DC. Metal particle size and structure of the metal-support interface of carbon-supported platinum catalysts as determined with EXAFS spectroscopy. *J Phys Chem B* 2004;108: 18509–19.
- [27] Zeng J, Lee JY. Effects of preparation conditions on performance of carbon-supported nanosize Pt–Co catalysts for methanol electro-oxidation under acidic conditions. *J Power Sources* 2005; 140:268–73.
- [28] Kawabuchi Y, Oka H, Kawano S, Mochida I, Yoshizawa N. The modification of pore size in activated carbon fibers by chemical vapor deposition and its effects on molecular sieve selectivity. *Carbon* 1998;36(4):377–82.
- [29] Harris PJF. Impact of the discovery of fullerenes on the carbon science. In: Radovic LR, editor. *Chemistry and physics of carbon*, vol. 28. New York: Marcel Dekker; 2003. p. 1–40.
- [30] Cundy CS, Cox PA. The hydrothermal synthesis of zeolites: history and development from the earliest days to the present time. *Chem Rev* 2003;103:663–702.
- [31] Sing KSW, Everett DH, Haul RAW, Moscou L, Pierotti RA, Rouquerol J, et al. IUPAC Recommendations 1984: reporting physisorption data for gas/solid systems with special reference to the determination of surface area and porosity. *Pure Appl Chem* 1985;57(4):603–19.
- [32] Li W, Liang C, Zhou W, Qiu J, Zhou Z, Sun G, et al. Preparation and characterization of multiwalled carbon nanotube-supported platinum for cathode catalysts of direct methanol fuel cells. *J Phys Chem B* 2003;107:6292–9.
- [33] Liu Z, Lee JY, Han M, Chen W, Gan LM. Synthesis and characterization of PtRu/C catalysts from microemulsions and emulsions. *J Mater Chem* 2002;12:2453–8.
- [34] Maruyama J, Sumino K, Kawaguchi M, Abe I. Influence of activated carbon pore structure on oxygen reduction at catalyst layers supported on rotating disk electrode. *Carbon* 2004;42(15): 3115–21.